1-1-1998

Generalized multiphoton-ionization cross sections of the rare gases for 500-fs, 248.6-nm pulses

Cornelis J. Uiterwaal
University of Nebraska - Lincoln, cuiterwaal2@unl.edu

D. Xenakis
Foundation for Research and Technology–Hellas, Institute of Electronic Structure & Laser, Laser and Applications Division, GR-711 10 Heraklion, Crete, Greece

D. Charalambidis
Foundation for Research and Technology–Hellas, Institute of Electronic Structure & Laser, Laser and Applications Division, GR-711 10 Heraklion, Crete, Greece

P. Maragakis
Max-Planck-Institut für Quantenoptik, Hans-Kopfermann-Strasse 1, D-85748 Garching, Germany

H. Schröder
Max-Planck-Institut für Quantenoptik, Hans-Kopfermann-Strasse 1, D-85748 Garching, Germany

See next page for additional authors

Follow this and additional works at: http://digitalcommons.unl.edu/physicsuiterwaal

Part of the Physics Commons

Authors

Cornelis J. Uiterwaal, D. Xenakis, D. Charalambidis, P. Maragakis, H. Schröder, and P. Lambropoulus

Generalized multiphoton-ionization cross sections of the rare gases for 500-fs, 248.6-nm pulses

C. J. G. J. Uiterwaal[1] [*], D. Xenakis[1], D. Charalambidis[1,2], P. Maragakis[3], H. Schröder[3], and P. Lambropoulos[1,2,3]

[1]*Foundation for Research and Technology–Hellas, Institute of Electronic Structure & Laser, Laser and Applications Division, P.O. Box 1527, GR-711 10 Heraklion, Crete, Greece*
[2]*Department of Physics, University of Crete, Crete, Greece*
[3]*Max-Planck-Institut für Quantenoptik, Hans-Kopfermann-Strasse 1, D-85748 Garching, Germany*
Received 16 June 1997

Absolute values for the generalized multiphoton-ionization cross sections and saturation intensities of rare gases are reported for 500-fs, 248.6-nm pulses. For He, Ar, and Kr these values are experimentally determined from the intensity dependence of the ponderomotive shift for intensities comparable to and above the saturation intensity. The measured experimental cross sections [$\sigma_{(5)}^{He}=(0.9_{+9}^{-0.4})\times10^{-152}$ cm^{10} s^4, $\sigma_{(4)}^{Ar}=(1.3_{+1}^{-0.5})\times10^{-116}$ cm^8 s^3, $\sigma_{(3)}^{Kr}=(1.2_{+1.7}^{-0.6})\times10^{-82}$ cm^6 s^2, $\sigma_{(3)}^{Xe}=(50_{-45}^{+350})\times10^{-82}$ cm^6 s^2] are found to be in good agreement with theoretical values [$\sigma_{(5)}^{He}=4.4\times10^{-152}$ cm^{10} s^4 (*ab initio*), $\sigma_{(4)}^{Ar}=1.1\times10^{-115}$ cm^8 s^3 (scaling), $\sigma_{(3)}^{Kr}=0.7\times10^{-82}$ cm^6 s^2 (scaling), $\sigma_{(3)}^{Xe}=5\times10^{-82}$ cm^6 s^2 multichannel quantum defect theory]. For Ne it is found that a single-rate description is not valid, and therefore the present model for the analysis of the experimental results cannot be applied. The reported Xe experimental cross sections are based on the conventional method of measuring the ion yield vs laser intensity with its concomitant reduced accuracy.

[*] Present address: Max-Planck-Institute für Quantenoptik, Hans-Kopfermann-Strasse 1, D-85748 Garching, Germany.

Generalized multiphoton-ionization cross sections of the rare gases for 500-fs, 248.6-nm pulses

C. J. G. J. Uiterwaal,[1,*] D. Xenakis,[1] D. Charalambidis,[1,2] P. Maragakis,[3] H. Schröder,[3] and P. Lambropoulos[1,2,3]

[1]*Foundation for Research and Technology–Hellas, Institute of Electronic Structure & Laser, Laser and Applications Division,*
P.O. Box 1527, GR-711 10 Heraklion, Crete, Greece
[2]*Department of Physics, University of Crete, Crete, Greece*
[3]*Max-Planck-Institut für Quantenoptik, Hans-Kopfermann-Strasse 1, D-85748 Garching, Germany*
(Received 16 June 1997)

Absolute values for the generalized multiphoton-ionization cross sections and saturation intensities of rare gases are reported for 500-fs, 248.6-nm pulses. For He, Ar, and Kr these values are experimentally determined from the intensity dependence of the ponderomotive shift for intensities comparable to and above the saturation intensity. The measured experimental cross sections $[\sigma_{(5)}^{He} = (0.9_{+9}^{-0.4}) \times 10^{-152}$ cm^{10} s^4, $\sigma_{(4)}^{Ar} = (1.3_{+1}^{-0.5}) \times 10^{-116}$ cm^8 s^3, $\sigma_{(3)}^{Kr} = (1.2_{+1.7}^{-0.6}) \times 10^{-82}$ cm^6 s^2, $\sigma_{(3)}^{Xe} = (50_{-45}^{+350}) \times 10^{-82}$ cm^6 s$^2]$ are found to be in good agreement with theoretical values $[\sigma_{(5)}^{He} = 4.4 \times 10^{-152}$ cm^{10} s^4 (*ab initio*), $\sigma_{(4)}^{Ar} = 1.1 \times 10^{-115}$ cm^8 s^3 (scaling), $\sigma_{(3)}^{Kr} = 0.7 \times 10^{-82}$ cm^6 s^2 (scaling), $\sigma_{(3)}^{Xe} = 5 \times 10^{-82}$ cm^6 s^2 multichannel quantum defect theory]. For Ne it is found that a single-rate description is not valid, and therefore the present model for the analysis of the experimental results cannot be applied. The reported Xe experimental cross sections are based on the conventional method of measuring the ion yield vs laser intensity with its concomitant reduced accuracy. [S1050-2947(98)00201-7]

PACS number(s): 32.80.Rm, 32.80.Fb, 32.80.Wr

I. INTRODUCTION

Atoms exposed to a strong electromagnetic field may undergo multiphoton ionization (MPI) [1]. If the applied field is strong enough, a series of peaks can be observed in the accompanying photoelectron spectra [2]. This phenomenon, known as above-threshold ionization (ATI), corresponds to the absorption of an integer number of photons above the ionization threshold, before the atom decays to an ion and a free electron.

According to lowest-order perturbation theory (LOPT), the rate dP/dt (s^{-1}) of an N-photon ionization process is

$$\frac{dP}{dt}(t) = [1 - P(t)]\sigma_{(N)}\Phi^N(t), \tag{1}$$

where $P(t)$ is the probability of finding the atom ionized at time t, $\sigma_{(N)}$ is the generalized N-photon ionization cross section (in cm^{2N} s^{N-1}) that, generally speaking, is intensity and thus time dependent, and $\Phi(t)$ is the photon flux as a function of time (in cm^{-2} s^{-1}). It will be convenient to write the photon flux as $\Phi(t) = \Phi_0 F(t)$, with Φ_0 the maximum photon flux (at time $t=0$) and $F(t)$ the (dimensionless) laser pulse temporal profile, normalized to $F(t=0)=1$. The ionization probability $P(t)$ at a time t in the laser pulse temporal evolution is given by the solution of Eq. (1) [3,4]:

$$P(t) = 1 - \exp\left(-\int_{-\infty}^{t}\sigma_{(N)}\Phi^N(t')dt'\right). \tag{2}$$

The description of a multiphoton-ionization process with a single rate as in Eq. (1) may in general be questionable if

_____

*Present address: Max-Planck-Institute für Quantenoptik, Hans-Kopfermann-Strasse 1, D-85748 Garching, Germany.

resonances with ac-Stark shifted atomic states take place during the temporal evolution of the laser pulse. Such dynamic resonances may cause an increase in the ionization rate at the moment they get populated, or may keep the population and ionize later in the pulse evolution, or they might even not ionize at all. In all such cases, it can be anticipated that a single rate will not describe the ionization process properly. The generalized cross section in such cases will become intensity and thus time dependent. If, however, the effect of resonances is to modify the cross section only slightly, or for a very short time, the convenient single-rate description can be maintained introducing an *effective* cross section that includes the smooth effects of dynamic resonances and thus describes the overall average behavior. For the case of an intensity-independent cross section $\sigma_{(N)}$ we find for the ionization probability after the pulse is completed (so for $t \to \infty$)

$$P(t \to \infty) = 1 - \exp(-\sigma_{(N)}\Phi_0^N t_{\text{eff}}), \tag{3}$$

in which we have introduced the effective pulse duration $t_{\text{eff}} = \int_{-\infty}^{\infty} F^N(t')dt'$.

For intensities far below saturation (so for $\sigma_{(N)}\Phi_0^N t_{\text{eff}} \ll 1$) Eq. (3) can be expanded to give

$$\ln P(t \to \infty) = N \ln\Phi_0 + \ln\sigma_{(N)} + \ln t_{\text{eff}} \tag{4}$$

and a log-log plot of measured ion yields vs laser intensity should therefore be a straight line. The detailed shape of such experimental log-log plots for intensities *above* the saturation intensity depends on whether or not interaction volume effects are eliminated by the experimental conditions [5,6]. One way to determine generalized MPI cross sections is to deduce saturation intensities from such log-log plots and then use the relation [cf. Eq. (9) below]

$$\sigma_{(N)} = (\hbar\omega/I_{\text{sat}})^N t_{\text{eff}}^{-1}. \tag{5}$$

The accuracy of this method, however, is limited by the large uncertainties in the precise value of I_{sat} that arise from the uncertainties in both the measurement of the size of the focal spot and hence in the intensity calibration, and in the determination of the exact value of I_{sat} from the experimental curve. The uncertainty in the intensity measurements is inherent even in elaborate models including spatiotemporal integration and fitting of the ion yield intensity dependence to the experimental data.

In a recent work [7], we utilized an alternative method to determine saturation intensities and effective generalized ionization cross sections. In the present work we describe an advanced modified version of the previous method that associates more accurately the measured quantities with the quantities given by the model. The method utilizes the laser intensity dependence of the ponderomotive shift as measured in ATI photoelectron spectra, for intensities above the saturation intensity. As is well known [8], the ionization threshold of an atomic system shifts up by the quiver energy of a free electron in the electromagnetic field of the laser, i.e., by the ponderomotive shift

$$
U_p = \begin{cases} \dfrac{(eE_0)^2}{4m\omega^2} = \dfrac{e^2}{2mc\varepsilon_0\omega^2}\,I & \text{(in SI units)} \\[3mm] \dfrac{2\pi\alpha}{\omega^2}\,I & \text{(in atomic units),} \end{cases} \tag{6}
$$

where e and m are the charge and the mass of the electron, E_0 is the electric field strength, I and ω are the intensity and the angular frequency of the laser, and α is the fine structure constant. This shift results in an equal shift of the photoelectron kinetic energy $E_{\text{kin}} = N\hbar\omega - IP - U_P$, with IP the unperturbed ionization threshold energy. As long as the laser pulse duration is short enough so that the electrons do not have the time to escape from the focus (in which case they would regain the lost energy through ponderomotive scattering, i.e., the acceleration caused by the field gradient) the shift is observable in the ATI spectra [9–11]. The determination of the laser intensity using measured ponderomotive shifts has been proposed earlier [12]. As our method relies on photoelectron kinetic energy measurements and not on laser intensity measurements, saturation intensities and effective generalized ionization cross sections can be found with an increased accuracy, of typically 15–25 % for saturation intensities, and of better than one order of magnitude for generalized cross sections.

The outline of this paper is as follows. After a brief description of the experimental setup, experimental ATI spectra will be presented, as well as MPI ion yield curves of He, Ne, and Ar. Next, a model will be presented that establishes a relation between (i) the detailed behavior of the maximum observed ponderomotive shift in ATI spectra as a function of laser intensity and (ii) the saturation intensity and thus the generalized cross section of the MPI process. Then, the effect of a pedestal in the laser pulse will be investigated. Finally, measured values of the saturation intensities and effective generalized ionization cross sections will be given for He, Ar, and Kr, and these values will be compared with theory. From the measured Ne-ion yield curve, we find that Ne MPI cannot be described as a single-rate process, and therefore a straightforward calculation of a saturation intensity and cross section for Ne cannot be performed.

II. EXPERIMENTAL SETUP

The experimental setup consisted of (i) a hybrid dye-excimer laser system [13] delivering pulses of $\sim$500-fs duration at a wavelength of $\sim$248 nm with a repetition rate of 4 Hz, a maximum energy of 14 mJ, and an amplified spontaneous emission (ASE) to pulse contrast ratio less than 10^{-6} at focus, and (ii) a magnetically shielded 20-cm-long photoelectron time-of-flight spectrometer operating at a background pressure of 10^{-9} mbar. The laser beam was focused with a 15-cm focal length lens into the spectrometer. All spectra are measured for laser intensities resulting in a Keldysh parameter γ [14] larger than unity. It is thus expected that MPI is dominating tunnel ionization [15]. Furthermore, the ponderomotive scattering is estimated to be less than 2% of the total ponderomotive shift for kinetic energies of the order of 10 eV. This is negligibly small and will thus not be considered in the following. It should be noted that we do not know the exact spatial pulse shape at the focus, so that this estimation is based on a conventional intensity distribution.

The Ar-ion yield versus laser intensity measurements were also performed with this spectrometer after changing the polarity of the MCP detector stage and applying a repelling voltage. The He- and Ne-ion yield versus laser intensity measurements have been performed with a four grid reflection time-of-flight spectrometer [5,6]. This instrument is capable of extracting ions from a certain confined volume in which ionization is eventually fully saturated. In this way, volume effects can be avoided, provided that the laser intensity is sufficient to saturate the confinement volume.

III. MEASURED ATI SPECTRA FOR He, Ne, Ar, AND Kr

We have measured ATI spectra for the noble gases He, Ne, Ar, and Kr. Typical ATI spectra for the case of Ne and Ar are shown in Figs. 1 and 2 (spectra for He can be found in Ref. [7]). With the exception of Ne, no strong evidence of abrupt changes in the cross section due to dynamical resonances [16–19] is visible in the spectra of the above-mentioned atoms, for the given laser parameters. This implies that the use of an effective generalized cross section seems justified. In the case of Ar a single sharp peak appears
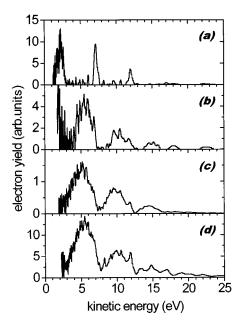
FIG. 1. ATI spectra of Ne for a selection of intensities. (a) 4.8 $\times 10^{14}$ W cm^{-2}, (b) 8.6$\times 10^{14}$ W cm^{-2}, (c) 1.1$\times 10^{15}$ W cm^{-2}, (d) 2.4$\times 10^{15}$ W cm^{-2}.

at a kinetic energy that is very close to the photoelectron kinetic energy in the zero-field limit [see the reduced part of Fig. 2(a)]. For the lowest intensities employed, only this sharp feature remains. This can be attributed to the fact that for Ar, the unperturbed energies of some states are very close to or at three-photon resonance within the laser bandwidth. For example, the closest match is the three-photon allowed $4d'[5/2]$, $J=3$ state at 14.972 eV, that falls within the three-photon energy of 14.96 ± 0.02 eV of the laser. However, it is
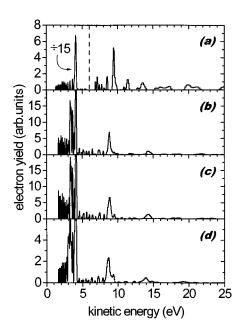

FIG. 2. ATI spectra of Ar for a selection of intensities. (a) 8.1 $\times 10^{13}$ W cm^{-2}—the part left of the dashed line has been reduced by a factor of 15 to show the sharp feature in the first photoelectron peak, (b) 1.5$\times 10^{14}$ W cm^{-2}, (c) 2.1$\times 10^{14}$ W cm^{-2}, (d) 2.3 $\times 10^{15}$ W cm^{-2}.
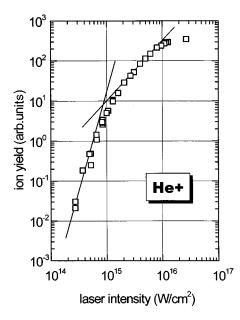

FIG. 3. Ion yield curve for He. To guide the eye, straight lines with slopes of 5 and $\frac{3}{2}$ are inserted.

only in the first photoelectron peak that this sharp feature appears and for higher intensities it is superimposed on a smooth structure. In the first ATI peak we see only this smooth structure that we used to determine the ponderomotive shift. The appearance of this smooth structure indicates that the ionization process does not saturate in the $(3+1)$ resonant scheme for the intensities employed here. This is also confirmed by the ion yield curve of Ar (see Fig. 5, and see below) that shows a slope of 4. In fact, assuming that the ac-Stark shift of the $4d'[5/2]$, $J=3$ state is ponderomotive, the three-photon resonance will no longer exist for intensities above $\sim 10^{12}$ W cm^{-2}, and a four-photon nonresonant process will become dominant. The presence of the sharp peak for all intensities could then be explained by the fact that in
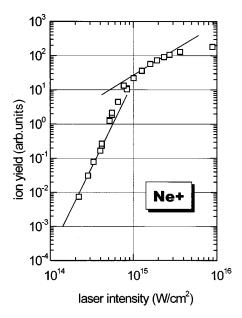

FIG. 4. Ion yield curve for Ne. To guide the eye, straight lines with slopes of 5 and $\frac{3}{2}$ are inserted.
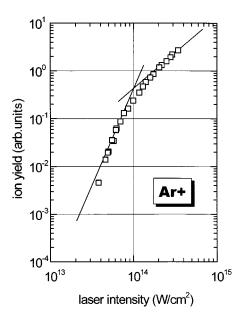
FIG. 5. Ion yield curve for Ar. To guide the eye, straight lines with slopes of 4 and $\frac{3}{2}$ are inserted.

FIG. 6. Measured ponderomotive shifts as a function of laser energy for He, Ne, Ar, and Kr. Some typical error bars are shown.

the tail of the temporal shape of the laser pulse the resonance will still exist. For the case of Ne, a richer structure appears in each ATI peak, and one clearly has to be more careful here. One way to see if any deviation of a single (effective) rate occurs is through inspection of a log-log plot of the ion yield as a function of intensity [cf. Eq. (4)]. In Figs. 3, 4, and 5 we give such plots that we have measured for He, Ne, and Ar. (In these three figures, we have inserted straight lines to guide the eye. In all cases, the well-known slope of 3/2 due to the volume effect is observed for the highest intensities measured. For He and Ne, which were measured in the spectrometer with a confined interaction volume, the last few datapoints show a stabilization of the ion yield, because for these intensities the whole confinement volume is saturated.) For He, a slope of 5 is found, and for Ar a slope of 4. These numbers are compatible with lowest-order perturbation theory when taking the ionization potential (IP) for these atoms in the low-intensity limit (negligible ponderomotive shift): for He, $IP = 24.58$ eV, and $5\hbar\omega = 24.94$ eV, and for Ar, $IP = 15.76$ eV, and $4\hbar\omega = 19.95$ eV. For He, channel closing will take place, since the maximum observed ponderomotive shift (see below) amounts to about 8 eV. The ion yield curve for He, on the other hand, does not give evidence of anything else but a single-rate process. Theoretical calculations of the He^+ yield versus laser intensity confirmed this five-photon ionization behavior [7]. For Kr, no ion yield curve is available, but in this case the maximum observed ponderomotive shift is only 0.4 eV, so channel closing can be excluded, and we assumed that MPI of Kr is a three-photon process ($3\hbar\omega = 14.96$ eV, and for Kr, $IP = 14.00$ eV). In fact, for Xe ($IP = 12.13$ eV), LOPT also predicts a three-photon process, and this has been confirmed previously through Xe^+-ion yield measurements using the same setup [6], supporting our assumption of a three-photon process for Kr.

Remarkably, the ion yield curve for Ne seems to indicate a deviation from single-rate behavior. Around the lowest measured intensities, we find a slope of 5.4 ± 0.4, compatible
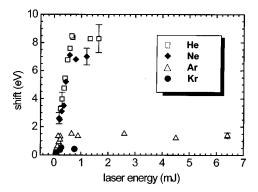
with LOPT ($5\hbar\omega = 24.94$ eV, and for Ne, $IP = 21.56$ eV). However, for intensities approaching the saturation intensity, the slope reaches a value of 6.4 ± 0.4. Clearly, Ne MPI is *not* a single-rate process in this context. Also, the Ne ATI spectra show clear structure, unlike the ATI spectra of He, Ar, and Kr, and very likely dynamical resonances play an important role here. The unperturbed energies of the four-photon allowed states of the $3p,3p'$ manifold of Ne are between 18.576 eV (for the $3p[5/2]$, $J = 2$ state) and 18.966 eV (for the $3p'[1/2]$, $J = 0$ state), whereas the energy level of the ground state dressed with four 248.6-nm photons is at 19.949 eV. Assuming that the ac-Stark shift of the $3p,3p'$ manifold is ponderomotive, we can expect these states to become resonant for intensities between 1.7×10^{14} and 2.4×10^{14} W cm^{-2}. In Fig. 4, the inflection in the Ne-ion yield curve occurs for an intensity of around 4×10^{14} W cm^{-2}, and taking into account an uncertainty in the intensity calibration of at least a factor of 2, we could possibly attribute the inflection to dynamical resonances with the angular momentum allowed states of the $3p,3p'$ manifold. Some of the structure observed in the ATI spectra of Ne could also be attributed to those resonances.

Measured ponderomotive shifts as a function of laser intensity are given for He, Ne, Ar, and Kr in Fig. 6. The ponderomotive shifts were determined from the ATI spectra by fitting a straight line through the low kinetic energy side of each ATI peak and determining the intersection of this straight line with the ordinate. As will be discussed in Sec. IV below, this method will give the maximum ponderomotive shift of an ATI peak, neglecting a small fraction q (in the order of 1%) of photoelectrons that has an even higher ponderomotive shift. The method employing the straight line has the following two disadvantages: (i) the position of the beginning of the peak can be determined with lower accuracy than the position of the top of the peak because of the lower signal-to-noise ratio and possible overlapping of broad ATI peaks, and (ii) the low kinetic energy side is more easily deformed by space charge effects so that space charge free conditions have to be rigorously established. Instead of using this method, one could decide to measure the shift of the top of each ATI peak, but the top of an ATI peak does not necessarily correspond to the highest intensity the atoms are exposed to, and might be affected by transient resonances or by volume effects, shifting it back to higher kinetic energies for high laser energies. Of course, in the special case of Ne
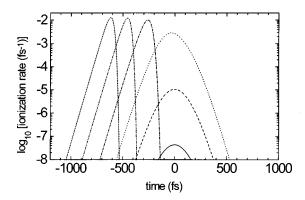
FIG. 7. Typical multiphoton ionization rate curves for a five-photon process with $\sigma_{(5)} = 1.0 \times 10^{-152}$ cm^{10} s^4, for a hyperbolic secant squared pulse with a FWHM of 500 fs ($I_{sat} = 6.8 \times 10^{14}$ W cm^{-2}), and for a photon energy $\hbar\omega = 4.99$ eV. Rate curves are shown for intensities that are 0.1 (—), 0.3 (------), 1 (···········), 3 (-·-·-·-·-), 10 (-·-·--·--·-), and 30 (·············) times the saturation intensity.

finding the tops of ATI peaks is meaningless due to the structure that is present in each ATI peak. For all measured elements in Fig. 6 the ponderomotive shift first increases linearly with laser energy up to a certain value that is determined by its specific atom. This maximum value corresponds to laser intensities above the ionization saturation intensity. For laser energies larger than this value the shift stabilizes to a constant value within the experimental error. From this maximum value of the ponderomotive shift ionization saturation intensities as well as generalized cross sections can be determined, as will be illustrated in the next section.

IV. PONDEROMOTIVE SHIFTS VS ENERGY

In this section we will show how the maximum ponderomotive shift that is observed in an ATI spectrum depends on laser energy, for intensities that are not small compared to the saturation intensity, and derive a theoretical expression for this dependence. Through comparison of this expression to experimental results we will find absolute values for the generalized MPI cross section and the saturation intensity. We start the discussion of the model by presenting (see Fig. 7) some typical curves showing the multiphoton-ionization rate as a function of time in for a selection of intensities below and above the saturation intensity. To calculate these example rate curves, we assumed a five-photon process ($N = 5$), and took a hyperbolic secant squared laser profile $F(t)$ with a full width at half maximum (FWHM) of 500 fs, a typical five-photon generalized cross section [7] of 1.0×10^{-152} cm^{10} s^4 ($I_{sat} = 6.8 \times 10^{14}$ W cm^{-2}), and a photon energy of 4.99 eV. These values were chosen to simulate MPI of He under our experimental conditions. Far below the saturation intensity the rate is essentially proportional to $F^N(t)$, since for this case the depletion of atoms (saturation) can be neglected (the factor $[1 - P(t)]$ in Eq. (1) is essentially equal to unity). For increasing intensities, at some point saturation will start playing a role, leading to rate profiles that are asymmetric, i.e., there is more ionization during the rising edge of the pulse than during the falling edge. For the high-
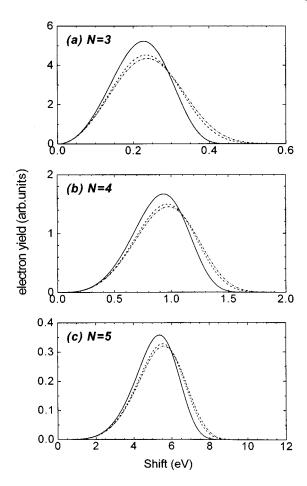

FIG. 8. Calculated electron yield curves $Y(U_p)$ as a function of the ponderomotive shift U_p for intensities above the saturation intensity. All curves were calculated for a hyperbolic secant squared pulse with a FWHM of 500 fs and for a photon energy $\hbar\omega = 4.99$ eV. The following numeric values were used for the generalized cross sections: (a) $N = 3$, $\sigma_{(3)} = 1.0 \times 10^{-82}$ cm^6 s^2, or $I_{sat} = 2.6 \times 10^{13}$ W cm^{-2}; (b) $N = 4$, $\sigma_{(4)} = 1.0 \times 10^{-116}$ cm^8 s^3, or $I_{sat} = 1.1 \times 10^{14}$ W cm^{-2}; (c) $N = 5$, $\sigma_{(3)} = 1.0 \times 10^{-152}$ cm^{10} s^4, or $I_{sat} = 6.8 \times 10^{14}$ W cm^{-2}. Electron yield curves are shown for intensities that are 3 (—), 10 (···········), and 100 (-·-·-·-·-) times the saturation intensity.

est intensities shown ionization will take place only during the rising edge of the pulse, as the ionization probability will now rapidly become unity before the peak of the pulse is reached (making the factor $[1 - P(t)]$ in Eq. (1) approach zero). Knowing the rate at each time during the pulse evolution, we can now calculate the ATI peak profiles, using the relation between ponderomotive shift U_P (in eV) and intensity I (in W cm^{-2}) for the wavelength of 248.6 nm used in our experiments [cf. Eq. (6)]:

$$U_P = 5.7 \times 10^{-15} I, \qquad (7)$$

where of course the relation between intensity and photon flux is given by $I = \Phi\hbar\omega$, with $\hbar\omega$ the photon energy (in J).

For intensities far below the saturation intensity, a sharp maximum shift (or minimum kinetic energy) appears in the ATI peak, corresponding to ionization at the maximum intensity at time $t = 0$. This minimum in kinetic energy appears because ionization at all other times will give a smaller pon-

deromotive shift. What happens above the saturation intensity is shown in Figs. 8(a)–8(c), where some typical calculated curves showing the electron yield $Y(U_p)$ as a function of the ponderomotive shift U_p are displayed (i.e., the probability of finding an electron with ponderomotive shift in the range $[U_P, U_P + dU_P]$ is $Y(U_P)dU_P$): in Fig. 8(a) for a three-photon process, in Fig. 8(b) for a four-photon process, and in Fig. 8(c) for a five-photon process. To calculate these curves, we employed the relation

$$Y(U_P) = \frac{dP}{dt}\left(t(U_P)\right)\left|\frac{dt}{dU_P}\right|,$$

where the dependence of t on U_P is given by the inverse of the laser pulse temporal profile. Since for an N-photon process the relation between the kinetic energy E_{kin} of the photoelectron and the ponderomotive shift U_P is $E_{kin} = N\hbar\omega - IP - U_P$, the calculated curves can be considered as ATI peak shapes that were mirrored in a vertical axis. In the calculations for these figures we used a hyperbolic secant squared laser pulse with a FWHM of 500 fs, and a 4.99-eV photon energy to simulate our experimental laser pulse, and the cross sections used were chosen to approach the experimentally determined values (see below) of Kr for $N=3$, of Ar for $N=4$, and of He for $N=5$. Peak shapes are given for intensities that are 3, 10, and 100 times the saturation intensity. These figures show that, for such intensities, again the electron yield will fall off rapidly for increasing shifts (or smaller kinetic energies), but in this case the maximum shift is *not* sharply defined. Although in this case the ensemble of atoms will already get depleted rapidly during the rising edge of the pulse (cf. Fig. 7), the probability for an atom *not* to be ionized at $t=0$ has a nonzero value of $1 - P(t=0)$, and this fraction of atoms will be exposed to the peak intensity of the pulse. However, if the intensity is high enough a ''saturation time'' τ_q can be found on the rising edge of the pulse, after which the ionization rate becomes so small because of saturation that the fraction q of electrons produced during the rest of the pulse (i.e., for $t > \tau_q$) can be safely ignored. For $\tau_q < 0$ this means that the atoms will effectively not be exposed to the maximum intensity $I(t=0) = I_0$, but instead the maximum intensity they will experience is $F(\tau_q)I_0$. Of course, for $\tau_q \geq 0$ the maximum intensity that atoms are exposed to *does* equal $I(t=0) = I_0$. In our previous publication [7], using the conventional definition of saturation, we chose $q = e^{-1} \approx 0.37$, corresponding to a ''saturation time'' $\tau_{1/e}$ given by $\sigma_{(N)}\Phi_0^N \int_{-\infty}^{\tau_{1/e}} F^N(t')dt' = 1$ [cf. Eq. (2)]. In the present work, however, we will use a value for q that is in closer accordance with the way the maximum ponderomotive shift is determined from our experimental spectra. We will see that this leads to a better agreement between the theoretical and experimental values of $\sigma_{(N)}$. To keep the formulas to be derived below as general as possible, we will postpone the determination of a proper value for q to the end of this section. For the moment we will just assume that the measured maximum ponderomotive shifts correspond to ionization at time $t = \tau_q$, where τ_q is found by solving $P(t=\tau_q) = 1 - q$, or equivalently for an intensity-independent $\sigma_{(N)}$ [cf. Eq. (2)]:

$$\sigma_{(N)}\left(\frac{I_0}{\hbar\omega}\right)^N \int_{-\infty}^{\tau_q} F^N(t')dt' = -\ln q. \tag{8}$$

To derive the relation between the ponderomotive shift and the generalized MPI cross section we will also need the usual definition of saturation intensity I_{sat}:

$$\sigma_{(N)}\left(\frac{I_{sat}}{\hbar\omega}\right)^N t_{eff} = 1. \tag{9}$$

Evidently, from Eqs. (8) and (9),

$$\frac{I_0}{I_{sat}} = \left(\frac{-(\ln q)t_{eff}}{\int_{-\infty}^{\tau_q} F^N(t)dt}\right)^{1/N}. \tag{10}$$

Using Eqs. (7), (8), and (10) we find for the maximum ponderomotive shift (at $t = \tau_q$) as a function of intensity I_0 [20]

$$U_p(I_0) = 9.1 \times 10^{-34}\hbar\omega \frac{1}{\sigma_{(N)}^{1/N}} \frac{\widetilde{U}_q(\widetilde{I})}{t_{eff}^{1/N}}, \tag{11}$$

with U_p and $\hbar\omega$ in eV, $\sigma_{(N)}$ in $cm^{2N} s^{N-1}$, and t_{eff} in s. The appearing dimensionless quantity $\widetilde{U}_q$ depends (for a given q) only on the normalized intensity $\widetilde{I} = I_0/I_{sat}$ and can easily be calculated for a given temporal shape of the laser pulse. Its definition being (for $\tau_q < 0$)

$$\widetilde{U}_q(\widetilde{I}) = F(\tau_q)\widetilde{I} = \frac{F(\tau_q)I_0}{I_{sat}}, \tag{12}$$

we see that it equals the ponderomotive shift occurring at time $t = \tau_q$ for intensity I_0, divided by the maximum ponderomotive shift at the saturation intensity [cf. Eq. (7)] and we can thus term it the normalized ponderomotive shift. With the use of Eq. (11) we can now express the generalized MPI cross section in terms of the measured ponderomotive shift $U_p(I_0)$ as

$$\sigma_{(N)} = \left(9.1 \times 10^{-34} \frac{\hbar\omega}{U_p(I_0)}\right)^N \frac{\widetilde{U}_q^N(\widetilde{I})}{t_{eff}}, \tag{13}$$

and the saturation intensity (in W cm^{-2}) as

$$I_{sat} = \frac{1.75 \times 10^{14} U_p(I_0)}{\widetilde{U}_q(\widetilde{I})}. \tag{14}$$

In general, we can determine absolute values for $\sigma_{(N)}$ and I_{sat} using Eqs. (13) and (14) by fitting the measured curve $U_p(I_0)$ to a calculated curve $\widetilde{U}_q(\widetilde{I})$. If a maximum value appears in the calculated and experimental curves, we can use these maxima in Eqs. (13) and (14). It will be sufficient to calculate $\widetilde{U}_q(\widetilde{I})$ for a single value of q, say for $q = e^{-1}$, because then the dependence of $\sigma_{(N)}$ and I_{sat} on q can be found as follows. Using Eq. (10), it can be easily shown that if for $q = e^{-1}$ the $\widetilde{U}_q(\widetilde{I})$ curve consists of the set of points $\{(\widetilde{I}_{1/e}, \widetilde{U}_{1/e})\}$, the $\widetilde{U}_q(\widetilde{I})$ curve for any other value of q con-
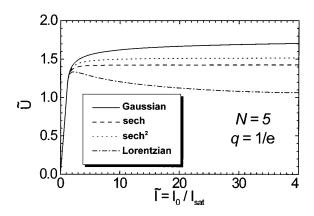
FIG. 9. Calculated curves of the normalized ponderomotive shift $\widetilde{U}_{1/e}$ as a function of normalized intensity $\widetilde{I}$ for four different laser temporal pulse shapes: Gaussian, hyperbolic secant, hyperbolic secant squared, and Lorentzian. The curves were calculated for $N=5$ and $q=1/e$. The FWHM of all four laser pulse shapes is 500 fs.
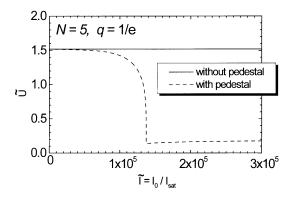

FIG. 10. The effect of a pedestal. The curve shows the normalized ponderomotive shift $\widetilde{U}_{1/e}$ as a function of normalized intensity $\widetilde{I}$ for a hyperbolic secant squared pulse with a FWHM of 500 fs, calculated for $N=5$ and $q=1/e$. Solid line: no pedestal, dashed line: with pedestal.

sists of the set of points $\{((-\ln q)^{1/N}\widetilde{I}_{1/e},(-\ln q)^{1/N}\widetilde{U}_{1/e})\}$. This means that if the $\widetilde{U}_{1/e}(\widetilde{I})$ curve has an (asymptotic) maximum, the $\widetilde{U}_q(\widetilde{I})$ curve also has an (asymptotic) maximum, and the value of this maximum will be $(-\ln q)^{1/N}$ times larger. In other words, we can replace $\widetilde{U}_q(\widetilde{I})$ in Eqs. (13) and (14) by $\widetilde{U}_{q=1/e}(\widetilde{I})(-\ln q)^{1/N}$, and thus we find that $\sigma_{(N)}$ scales with q as $(-\ln q)$ and I_{sat} as $(-\ln q)^{-1/N}$. This implies that reliable values for $\sigma_{(N)}$ and I_{sat} can be found using any reasonable estimation of just the order of magnitude of q.

In Fig. 9 we show calculated curves of $\widetilde{U}_{1/e}(\widetilde{I})$ for four different temporal pulse shapes: Gaussian, hyperbolic secant, hyperbolic secant squared, and Lorentzian. The curves were calculated for $N=5$. Calculations for $N=4$ and 3 give very similar curves. The figure shows that for a hyperbolic secant or a hyperbolic secant squared pulse the normalized shift reaches asymptotically a constant highest value. The curve for the Gaussian pulse shows a slowly increasing behavior for increasing intensities, whereas the Lorentzian curve passes through a maximum.

In the following we will use a hyperbolic secant squared laser pulse shape with a FWHM of 500 fs, as this fits best to measured autocorrelation traces. For this pulse shape, with $N=5$, the (asymptotic) maximum value of $\widetilde{U}_{1/e}(\widetilde{I})$ equals 1.52 and $t_{eff}=230.5$ fs. For $N=4$ we find $[\widetilde{U}_{1/e}(\widetilde{I})]_{max}=1.64$ and $t_{eff}=259.3$ fs, and for $N=3$ these values are $[\widetilde{U}_{1/e}(\widetilde{I})]_{max}=1.85$ and $t_{eff}=302.6$ fs.

Finally, we must determine a value for q. In the analysis procedure of our experimental data, we take a straight line passing through the low kinetic energy part of an ATI peak that is above the noise level, and determine the intersection of this straight line with the ordinate in order to find the maximum shift. Applying this procedure to some typical theoretically calculated ATI peak shapes, like the ones appearing in Fig. 8, we can estimate a value for q. We found for $N=5$ a fraction of neglected electrons $q\approx0.012$ ($-\ln q\approx4.4$), for $N=4$ we found $q\approx0.015$ ($-\ln q\approx4.2$), and for $N=3$ we found $q\approx0.018$ ($-\ln q\approx4.0$). However, in the experiment space charge effects, volume effects, and possible resonances may affect the ATI peak shape. Pressure-

dependent measurements have ruled out space charge effects in the measured shifts. Volume effects are expected to modify only the higher kinetic energy side of each peak, and are thus not expected to influence the result dramatically. One could imagine one scenario where the occurrence of a dynamic resonance would influence the fraction q. In this scenario a state dynamically shifts into resonance, becomes populated, and then remains populated for a considerable fraction of the pulse duration while undergoing a downward ac-Stark shift, and photoionizes at a later stage of the pulse evolution. If this were to happen, the ponderomotive shift of the ionization threshold would be overestimated for intensities high enough to cause such dynamic resonances. However, for the low-intensity part of Fig. 6 the measured shifts as a function of laser energy are in accordance with Eq. (7) (for intensities with $\tau_q>0$), all datapoints lying within the error on a straight line, even for Ne, where the presence of resonances seems obvious. Apparently, the part of the ATI peaks that we use to determine the shift is not affected too much by the presence of resonances.

Anyway the precise value of q is not very important, since only the order of magnitude of q plays a role, so that our method gives reliable results.

V. THE EFFECT OF A PEDESTAL

In this section the influence of a pedestal in the laser pulse temporal profile will be discussed. Short laser pulses are produced by several types of compression of initially longer pulses. The production of short and strong pulses requires amplification stages of an initially weak pulse. The compression and amplification procedures may introduce low-intensity but long duration pedestals on which the short pulse is superimposed. The presence of such pedestals may strongly affect the results of experiments and produce artifacts. For example, in MPI experiments in the presence of a broad pedestal, ionization may already saturate before the atom is exposed to the actual short pulse. A pedestal is present in our laser pulses due to amplified spontaneous emission (ASE) in the laser system, the width of which is similar to that of the gain profile of the final KrF amplifying excimer, and thus is on the order of a few ns. For high

TABLE I. Experimental and theoretical values of the generalized MPI cross sections $\sigma_{(N)}$ for the noble gases He, Ne, Ar, Kr, and Xe. *Ab initio* results for He [labeled time-dependent Schrödinger equation (TDSE) and TDHF] taken from Ref. [7]. For comparison, an experimental value of $\sigma_{(3)}^{Xe}$ is shown, calculated with Eq. (5) using the saturation intensity taken from the Xe-ion yield curve given in Ref. [6], with errors including uncertainties in the intensity calibration. The multichannel quantum defect theory (MQDT) theoretical value for Xe is also taken from Ref. [6].

Method	$\sigma_{(5)}^{He}$ ($cm^{10}\ s^4$)	$\sigma_{(5)}^{Ne}$ ($cm^{10}\ s^4$)	$\sigma_{(4)}^{Ar}$ ($cm^8\ s^3$)	$\sigma_{(3)}^{Kr}$ ($cm^6\ s^2$)	$\sigma_{(3)}^{Xe}$ ($cm^6\ s^2$)
Experiment	$(0.9_{+9}^{-0.4}) \times 10^{-152}$	?	$(1.3_{+1}^{-0.5}) \times 10^{-116}$	$(1.2_{+1.7}^{-0.6}) \times 10^{-82}$	$(50_{-45}^{+350}) \times 10^{-82}$
Scaling	8×10^{-152}	4×10^{-151}	1×10^{-115}	0.7×10^{-82}	2×10^{-82}
TDSE	14×10^{-152}				
TDHF	4.4×10^{-152}				
MQDT					5×10^{-82}

intensities, the presence of such a broad pulse might lead to saturation of ionization before the narrower principal pulse has ever started. At focus, our laser pulse has an ASE to pulse contrast ratio of better than $1:10^6$. Taking a worst case scenario, we will demonstrate now the effect of a 10-ns-wide Gaussian pedestal that has a 10^6 times smaller intensity than the principal 500-fs-wide pulse. In other words, the normalized laser pulse temporal profile $F(t)$ defined just below Eq. (1) consists now of the sum of two profiles with the above-mentioned widths: $F(t) = F_{principal}(t) + F_{ASE}(t)$, and we take $F_{ASE}(t=0) = 10^{-6} F_{principal}(t=0)$. In Fig. 10 we show for a five-photon process the normalized ponderomotive shift vs normalized laser intensity, calculated again for a hyperbolic secant squared laser pulse. From this figure, we see that the pedestal would play a role only for extremely large intensities, in the order of 10^5 times the saturation intensity. For such high intensities, saturation of ionization occurs already in the rising edge of the pedestal, and this effect lowers the ponderomotive shift dramatically, by about 90%. As expected from this figure, we observe no such drop in the ponderomotive shift, and we can therefore ignore the presence of ASE in our laser pulse for the present experiment.

VI. SATURATION INTENSITIES AND GENERALIZED CROSS SECTIONS FOR He, Ar, AND Kr

The model presented in Sec. IV is applied to the experimental data in Fig. 6 for He, Ar, and Kr. For our photon energy of $\hbar\omega = 4.99$ eV, the order of the MPI process for He is $N=5$, for Ar we have $N=4$, and for Kr $N=3$. The maxima of the observed shifts are for He (8 ± 1) eV, for Ar (1.4 ± 0.2) eV, and for Kr (0.4 ± 0.1) eV. For the saturation intensities of these noble gases we find the following values: $I_{sat,He} = (6.9\pm0.8)\times10^{14}$ W cm^{-2}, $I_{sat,Ar} = (1.0\pm0.15)$ $\times10^{14}$ W cm^{-2}, and $I_{sat,Kr} = (2.4\pm0.6)\times10^{13}$ W cm^{-2}. The values for the generalized cross sections are summarized in Table I, together with theoretical values based on a scaling law [3,4]. For He, we also give results of *ab initio* calculations from Ref. [7]. For comparison, an experimental value of $\sigma_{(3)}^{Xe}$ is shown as well that was calculated with Eq. (5) using the saturation intensity taken from the measured Xe-ion yield curve given in Ref. [6]. The errors given for this Xe value include uncertainties in the intensity calibration. For Xe, we also give a theoretical value taken from Ref. [6]. In all three cases (He, Ar, Kr) good agreement is found, the

experimental values being within one order of magnitude in agreement with the theoretical values. In the case of He, where fully *ab initio* calculations are available, the measured cross section value is in excellent agreement with the value calculated using the time-dependent Hartree-Fock (TDHF) approach, that is only a factor of 5 larger, and lies within the experimental error. To put this difference in a more familiar perspective, we should note that a five-photon generalized cross section is the square of an effective five-photon dipole matrix element. A difference of a factor of 5 is thus equivalent to a difference of $5^{1/10}$ or 17% in a dipole matrix element in a single-photon transition. For the special case of Ne, where we found that a single-rate description does *not* apply, a maximum shift for Ne of (7 ± 0.7) eV is observed, but here our model cannot be uniquely applied to calculate saturation intensity and cross section values.

VII. CONCLUSIONS

In this work, an alternative method for the determination of saturation intensities and effective generalized ionization cross sections in nonresonant MPI is presented in an improved version. An application to He, Ar, and Kr is presented. As the method relies on photoelectron kinetic energy measurements and not on laser intensity measurements, saturation intensities and effective generalized ionization cross sections can be found with an accuracy of typically better than 30% for saturation intensities, and of better than one order of magnitude for generalized cross sections. Our method cannot be rigorously applied to Ne, because measurements of the Ne$^+$ ion yield vs laser intensity indicate that MPI of Ne at 500 fs and 248.6 nm deviates from the behavior of a single-rate process. The results obtained enable the detailed testing of theoretical models and supply important atomic data to analytical techniques utilizing MPI.

[1] G. S. Voronov and N. B. Delone, Zh. Eksp. Teor. Fiz. Pis'ma Red. **1**, 42 (1965) [JETP Lett. **1**, 66 (1965)].

[2] P. Agostini, F. Fabre, G. Mainfray, G. Petite, and N. K. Rahman, Phys. Rev. Lett. **42**, 1127 (1979).

[3] P. Lambropoulos, Comments At. Mol. Phys. **20**, 199 (1987), and references therein.

[4] P. Lambropoulos and X. Tang, J. Opt. Soc. Am. B **4**, 821 (1987).

[5] M. Wagner and H. Schröder, Int. J. Mass Spectrom. Ion Processes **128**, 31 (1993).

[6] D. Charalambidis, P. Lambropoulos, H. Schröder, O. Faucher, H. Xu, M. Wagner, and C. Fotakis, Phys. Rev. A **50**, R2822 (1994).

[7] D. Charalambidis, D. Xenakis, C. J. G. J. Uiterwaal, P. Maragakis, Jian Zhang, H. Schröder, O. Faucher, and P. Lambropoulos, J. Phys. B **30**, 1467 (1997).

[8] R. R. Freeman and P. H. Bucksbaum, J. Phys. B **24**, 325 (1991), and references therein.

[9] T. S. Luk, T. Graber, H. Jara, U. Johann, K. Boyer, and C. K. J. Rhodes, J. Opt. Soc. Am. B **4**, 847 (1987).

[10] H. G. Muller, H. B. van Linden van den Heuvell, P. Agostini, G. Petite, A. Antonetti, M. Franco, and A. Migus, Phys. Rev. Lett. **60**, 565 (1988).

[11] M. D. Perry, A. Szoke, and K. C. Kulander, Phys. Rev. Lett. **63**, 1058 (1989).

[12] M. D. Perry and L. O. Landen, Phys. Rev. A **38**, 2815 (1988).

[13] S. Szatmari and F. P. Schäfer, Opt. Commun. **68**, 196 (1988).

[14] L. V. Keldysh, Zh. Eksp. Teor. Fiz. **47**, 1945 (1964) [Sov. Phys. JETP **20**, 1307 (1965)].

[15] E. Mevel, P. Breger, R. Trainham, G. Petite, P. Agostini, A. Migus, J.-P. Chambaret, and A. Antonetti, Phys. Rev. Lett. **70**, 406 (1993).

[16] R. R. Freeman, P. H. Bucksbaum, M. Milchberg, S. Darack, D. Schumacher, and M. E. Geusic, Phys. Rev. Lett. **59**, 1092 (1987).

[17] P. Agostini, P. Breger, A. L'Huillier, H. G. Muller, G. Petite, A. Antonetti, and A. Migus, Phys. Rev. Lett. **63**, 2208 (1989).

[18] H. Rottke, B. Wolff, M. Brickwedde, D. Feldmann, and K. H. Welge, Phys. Rev. Lett. **64**, 404 (1990).

[19] H. Rudolph, X. Tang, H. Bachau, P. Lambropoulos, and E. Cormier, Phys. Rev. Lett. **66**, 3241 (1991).

[20] Note that τ_q is a function of I_0 [cf. Eq. (8)].